Quantitative T2 changes and susceptibility weighted magnetic resonance imaging in the murine pregnancy

U. Krishnamurthy[1,2], G. Szalai[3], J. Neelavalli[1,2,*], Y. Shen[1], T. Chaiworapongsa[3,4], E. Hernandez-Andrade[3,4], N.G. Than[3,4], Z. Wu[3], L.Yeo[3,4], E. M. Haacke[1,2], R. Romero[3,5,6,*]

[1]Department of Radiology, Wayne State University School of Medicine, Detroit, Michigan, USA; [2]Department of Biomedical Engineering, Wayne State University College of Engineering, Detroit, Michigan, USA; [3]Perinatology Research Branch, NICHD/NIH/DHHS, Bethesda, Maryland, and Detroit, Michigan, USA; [4]Department of Obstetrics and Gynecology, Wayne State University School of Medicine, Detroit, Michigan, USA. [5]Department of Obstetrics and Gynecology, University of Michigan, Ann Arbor, MI; [6]Department of Epidemiology and Biostatistics, Michigan State University, East Lansing, MI, USA.

*****correspondence:

Roberto Romero, MD, D.Med.Sci

Perinatology Research Branch, NICHD, NIH, DHHS
Wayne State University, Hutzel Women's Hospital
3990 John R Street
Detroit, MI 48201, USA
Phone: +1 (313) 993-2700; Fax: +1 (313) 993-2694
E-mail: romeror@mail.nih.gov

Jaladhar Neelavalli, PhD

Department of Radiology
Wayne State University School of Medicine
4201 St. Antoine
Detroit, MI 48201, USA
Phone: +1 (313) 993-8610; Fax: +1 (313) 745-9182
Email: jneelava@med.wayne.edu

Short Title: Placental T2 changes and SWI

Abstract

Objective: Evaluating gestational age-dependent changes in T2 relaxation time in normal murine placentas in-vivo. Role of Susceptibility Weighted Imaging (SWI) in visualization of murine fetal anatomy was also elucidated.

Methods: Timed-pregnant CD-1 mice at gestational days (GD) 12 and 17 underwent magnetic resonance imaging (MRI). Multi echo spin-echo and SWI data were acquired. Placental T2 values at GD 12 and 17 were quantified. To account for the influence of systemic maternal physiologic factors on placental perfusion, maternal muscle was used as reference for T2 normalization. A linear mixed effects-model was used to fit the normalized T2 values and significance of the coefficients was tested. Fetal SWI images were processed and reviewed for venous vasculature and skeletal structures.

Results: The average placental T2 value decreased significantly on GD17 (40.17±4.10 msec) compared to that on GD12 (55.78±8.13 msec). The difference in normalized T2 values also remained significant (p=0.001). Using SWI, major fetal venous structures like the cardinal vein, subcardinal vein and portal vein etc., were visualized on GD12. In addition, fetal skeletal structures could also be discerned on GD17.

Conclusion: The T2 value of normal murine placenta decreases with advancing gestation. SWI demonstrated clear visualization of fetal venous vasculature and bony structures.

Key Words: Transverse relaxation (T2) time, SWI, venography, MRI, murine embryo

Introduction:

The chorioallantoic placenta is a highly vascularized organ that forms the interface between the maternal and fetal circulations in eutherian mammals. The extent of the feto-maternal contact varies widely among mammals depending on the type of placental interface, feto-maternal interdigitation, and placental shape [1, 2]. Besides its barrier function, the placenta facilitates directional nutrient, gas and waste product transport between the mother and her offspring. Moreover, the placenta is a rich source of fetal hormones, growth factors and cytokines that modulate maternal metabolism and immune functions. Therefore, the normal functioning placenta plays a pivotal role in supporting embryonic and fetal development, maternal-fetal immune tolerance, and the maintenance of pregnancy [3-9]. Placental dysfunction may lead to various clinical phenotypes, such as intrauterine growth restriction (IUGR), delivery of small-for-gestational age (SGA) neonates, preterm birth, and preeclampsia [9-14]. A growing body of evidence supports the concept that IUGR may be due to decreased utero-placental blood flow and subsequent chronic hypoxia and/or ischemia-reperfusion injury of the placenta, as well as reduced placental transport function [15-17]. Murine models are commonly used to understand and mimic the mechanisms of disease in human obstetrical syndromes, such as preeclampsia, IUGR and preterm birth [18-21]. Although, mice have hemochorial placentation, some structural and functional aspects are different compared to humans [1, 5]. For example, murine placenta contains three major zones: 1) maternal decidual zone; 2) Junctional zone, where maternal and fetal cells intermingle; and 3) Inner labyrinthine zone, where gas and nutrient exchange occur [5]. The latter zone is equivalent to the villous placenta in humans. Yet, in spite of these anatomical differences, the molecular mechanisms of placental gas and nutrient transport overlap in these species [5, 8, 22, 23], and thus, murine models can be employed to investigate changes in fetal growth and placental function in complications of human pregnancy.

Magnetic resonance imaging (MRI) based transverse relaxation (T2) time has been shown to correlate with the micro-vascular perfusion status of human tissue, and is sensitive to changes in perfusion and tissue morphology [24, 25]. The placental T2 relaxation time has potential to be a non-invasive biomarker for IUGR in both human and animal models [12, 26]. The T2 relaxation time is sensitive to blood volume and local tissue characteristics such as water diffusion and blood oxygenation [27, 28]. Prior MRI studies conducted in animal models have

used dynamic contrast enhanced (DCE) MRI to assess the functional behavior of the placenta [29-31]; however, this is not feasible in humans due to concerns about contrast agent use during pregnancy. Quantitative T2 relaxation time is sensitive to placental hypoxia in pregnancy complications (in both human and animal models) [26, 32]. Yet, human studies have shown that placental T2 relaxation time could change physiologically at different gestational ages [26, 33], which may also be the case in the murine pregnancy. Therefore, knowledge of the normal progression of placental T2 relaxation times at different gestational ages is necessary to understand changes occurring in various pathological conditions in animal models. In this study, we aimed to evaluate normal changes in T2 relaxation time of the murine placenta at two different gestational days (GD) (12 and 17).

Another key area of investigation is fetal vasculature, which is among the first systems to develop during embryonic life [34]. MRI examination of smaller structures (especially vascular), adds value in understanding fetal development [35], detecting phenotypes when using genetically engineered models, [36] and, assessment of the functionality in normal and pathological conditions [37-39]. Yet, in order to visualize and perform quantitative analysis of these structures, advanced imaging sequences are necessary. Visualization of small structures is largely limited not only by imaging resolution, but also by the lack of sufficient contrast. It is anticipated that susceptibility induced phase variations between the venous vasculature and background tissue might augment this contrast [40, 41]. Susceptibility Weighted Imaging (SWI) is a high-resolution, flow-compensated, blood-oxygen-level dependent (BOLD) based gradient echo (GRE) acquisition, which uses MR phase data to enhance tissue contrast based on the local differences in their magnetic susceptibility [42-44]. SWI images are more sensitive to the BOLD signal due to the unique combination of T2* weighted magnitude data with phase data. The phase images utilize the paramagnetic deoxy-hemoglobin as an endogenous contrast agent to enhance visualization of the venous structures [45]. Therefore, SWI phase images have value in visualizing and distinguishing bony structures, which are diamagnetic in nature, from paramagnetic venous structures [46]. SWI has been extensively used as a venographic technique in adult humans, and has evolved to be used in pediatric [47, 48] and neonatal venography [49]. More recently, this technique has also been used to visualize the venous vasculature of the fetal brain [50], and to highlight fetal micro bleeds and intracranial hemorrhage during pregnancy

[51]. In this study, we report our preliminary experience with SWI based MR venography to visualize the fetal venous vasculature in the normal murine pregnancy.

Materials and Methods

Animal care and handling

The study protocol was approved by the Institutional Animal Care and Use Committee (IACUC) at Wayne State University. Animal care and handling followed the standards set forth by the National Research Council of the National Academies [52]. Timed-pregnant CD-1 mice (n=7) were obtained from Charles River Laboratories (Wilmington, MA). Pregnancy was confirmed by manual examination on GD12. Mice were kept separately in filter top rodent cages and fed with *ad libitum* water and food. A regular 12:12 hour dark-light cycle and constant temperature (24±1ºC) and humidity (50±5%) were maintained in the animal room, and mice were monitored for food and water intake, vital signs, behavior and activity.

Imaging procedures

All MRI studies were performed on a 7.0T, 20 cm bore superconducting magnet (ClinScan, Bruker, Karlsruhe, Germany) interfaced with a Siemens console. Prior to image acquisition, anesthesia was induced by isoflurane (4% v/v) in an induction chamber to sedate the animals, and mice were kept under anesthesia (2% v/v isoflurane) throughout the acquisition time. The MRI studies consisted of three major sequences which followed the localization scans: 1) T2-weighted turbo spin echo (TSE) for anatomical evaluation; 2) multi-echo spin echo for T2 mapping; and 3) SWI for venography. A series of localization scans in different anatomical planes were first obtained following which T2-weighted TSE data were acquired for anatomical assessment of the fetus and for visualization of each corresponding placenta. A fat-saturated, multi echo T2-weighted spin echo sequence was used for the T2 measurement, which was acquired using the following sequence parameters: matrix size of 160 x 320; repeat time (TR) between 2540-2850 milliseconds (ms); slice thickness of 0.7/0.8mm; in-plane resolution of (0.08-0.13) x 0.13 mm^2,and a pixel bandwidth of 130 Hz/pixel. A total of six echoes [at echo times (TE) of 15, 30, 45, 60, 75, 90 ms or TEs of 10.8, 21.6, 32.4, 43.2, 54, 64.8 ms] were acquired, and T2 maps were generated using a custom code written in Matlab (MathWorks, Natick, MA). For venography evaluation, a 2D gradient echo SWI sequence was employed. The parameters used for SWI imaging were: TE of 7.84/5.42ms; TR between 600-850ms; acquisition matrix of 512 x 512; resolution of 0.08 x 0.08 x 0.7/0.8 mm^3; and bandwidth of 150Hz/pixel. MR

imaging parameters are summarized in Table 1. The maximum total acquisition time for the SWI sequence was 14.5 minutes. Both T2 and SWI images were acquired in an axial orientation relative to the magnetic axis.

Image processing

T2 maps were generated using the multi-echo data by fitting the signal to an exponential function on a pixel by pixel basis. Pixels with poor fit or those which resulted in negative values were threshold to zero. A free hand drawn region of interest (ROI) was used to map the placenta and the T2 values were recorded. Since measurements were carried out from more than one pregnant mouse at a given gestational age normalization was performed, to account for any systemic maternal physiologic factor that could influence placental T2 values. Normalization of the placental T2 values with the T2 value of a reference maternal tissue was used. In this case, maternal muscle tissue was selected as the reference region [53], Thus, the ratio was computed as placental T2 value / maternal-muscle T2 value.

For visualization of venous structures, the SWI phase images were first unwrapped using the prelude function in FMRIB's Software Library software (FSL) [54]. Following this, the unwrapped images were filtered using a homodyne filter [55] to remove any background low spatial frequency phase variation. These processed phase images were then multiplied onto the original magnitude images to create the SWI images [56]. The SWI phase images were reviewed for vasculature and bony structures.

Statistical analyses

A linear mixed effects-model was used to fit the normalized placental T2 values as a function of the group variable. Therefore, measurements within each animal were treated as correlated data, while accounting for the different number of data points within each animal. Significance of the coefficient was extracted from the fitted model using the *nlme* package [57] under the R statistical environment (www.r-project.org). A $p<0.05$ was considered significant.

Results

T2 relaxation times

On GD12, the T2 values from 26 placentas were measured from three pregnant mice while on GD17, the T2 values from 16 placentas were measured from four pregnant mice. The distribution of number of placentas/mouse was as follows: a) 5, 10 and 11 placentas respectively from the

three mice at GD12; b) 2, 3, 5 and 5 placentas respectively from the four mice at GD17. The average T2 value, measured across all placentas, was 55.78±8.13 msec (mean ± standard deviation) on GD12 and 40.17±4.10 msec on GD17 (Figure 1) (standard deviations represent the variation of the measured T2 value from one placenta to another). The maximum standard error of the mean in individual T2 measurements was 1.14msec, which is much smaller than the inter-placental T2 variation. The normalized T2 ratio for GD12 was 1.59±0.14 arbitrary units (a.u.), and was 1.13±0.13 a.u. for GD17 (Figure 2). The decrease in the normalized ratio values between GD12 and GD17 was statistically significant ($p=1.7x10^{-3}$). This indicates that the difference in T2 values between GD12 and GD17 is significant and not influenced by systemic differences in maternal physiology from one pregnant mice to another.

SWI venography

The processed SWI magnitude data shows a clear distinction between the three regions of the placenta: the labyrinth, junctional zone, and maternal decidua on GD17. Heterogeneity of the placenta may be visualized even at an early gestational age (e.g. GD12) (Figure 3). This heterogeneous signal was not very evident in the T2 weighted images or T2 maps. The processed phase images show the major veins due to the presence of deoxy-hemoglobin, which acts as an intrinsic contrast agent. For example, on GD12, the cardinal vein, vena cava, primary head vein, portal vein, and subcardial vein could be clearly visualized (Figures 4 and 5). The umbilical arteries, as well as vascular organs such as the heart and placenta were also visualized (Figures 4 and 5). In addition to most of these structures, the well-developed lobes of the lung were also visualized on GD17 (Figure 6). Development of bony structures in the murine embryo by GD17 leads to increased contrast of such structures on phase images, and could be distinguished easily from veins due to their diamagnetic phase signature [58]. Figure 7 shows murine bony structures, such as the ribs and vertebral body.

Discussion:

Principal findings of the study: 1) Placental T2 values decrease with advancing gestational age in the murine pregnancy, corresponding to normal physiological changes; 2) Gradient echo T2* based images can distinguish distinct layers within the placenta beginning in mid-gestation (GD12); and 3) using SWI, fetal venous vasculature and bony structures can be visualized without using exogenous contrast agents.

T2 – transverse relaxation time of the murine placenta:

The T2 relaxation time in MRI is known to be sensitive to microenvironment and metabolic changes [25, 27, 28, 59]. Previous reports in animal models have demonstrated the utility of the T2 transverse relaxation time in IUGR, mostly in late gestation [32]. The study herein was aimed at assessing the baseline T2 relaxation time values in normal murine placentas and their relationship with gestational age. Such knowledge is necessary when evaluating such values in conditions associated with placental pathology. The decreasing trend in T2 relaxation time with advancing gestation shown in the current study is consistent with what has been reported for human placenta [26, 33]. In general, decreased T2 relaxation time values of a tissue can be attributed to one or more of the following factors: 1) increase in the local deoxyhemoglobin concentration [27, 60]; 2) increase in the blood volume fraction [27, 60, 61]; 3) variations in blood flow [62]; 4) changes in the diffusion characteristics of the tissue micro-environment [27, 60, 61]; and/or 5) morphological changes within the tissue itself. In addition, changes in maternal physiology may influence placental vascularization, perfusion and growth, and have an impact on placental T2 relaxation values. Therefore in the study herein, we normalized the placental relaxation times by using maternal muscle tissue as an internal reference. Yet, a statistically significant difference remained in normalized placental T2 values. Blood supply to fetuses can vary in the same dam, depending on their location within the uterine horn [63]. This could be a contributing factor for the variation/standard deviation in placental T2 values for a given gestational age. With regard to general applicability of the results to other strains of mice (for example C57B16), we anticipate that the general trend of decreasing T2 with gestational age would be observed in them as well since placental perfusion characteristics are seen to evolve with gestational age. Nevertheless, due to the differences in vascular densities and tissue morphology between different strains of mice [64], the absolute T2 values may be different.

The murine placenta is heterogeneous and is composed of different regions: labyrinth, junctional zone, and decidua. T2 (or) R2 (=1/T2) maps of the placenta have been shown to distinguish between these regions at later gestational ages [32]. By using gradient echo T2* based images, we have shown that these regions can be visualized distinctly even in mid-gestation (GD12). The ability to distinguish various layers within the placenta is important, since such regions could be affected differently when there is placental pathology [32].

SWI venography of the murine placenta:

Traditionally, visualization of embryonic vascular development using MRI is accomplished using external contrast agents [65, 66], usually in the *ex vivo* setting [66-68]. More recently, high resolution three dimensional (3D) imaging based on T2* differences as exogenous contrast have been applied to highlight such vasculature [36, 69]. In the current study, we report the use of SWI phase images to create venograms/skeletal reconstruction of the murine fetus. Phase images have the distinct advantage of high signal to noise ratio (SNR) [70, 71] as compared to the magnitude MR images. The existence of huge susceptibility differences and the perturbation of the phase beyond the vessel wall enables detection of sub-voxel structures [72]. Due to these features, SWI, which uses both magnitude and phase images, can be used as an alternative to image the developing venous vasculature of the fetus. Phase information also allows distinction between veins and bony structures, because veins have a paramagnetic phase signature, while bones, (due to the presence of calcium) are diamagnetic in nature. SWI can also potentially be used for quantifying oxygen saturation in venous blood [73, 74].

MR Imaging of small structures is a tradeoff between resolution, field of view and acquisition time. In the study herein, we limited the SWI acquisition time to 14.5 minutes, which did not allow isotropic acquisitions. While the in-plane reconstructed resolution was 0.08mm, the slice thickness was 0.8mm. This highly asymmetric voxel size was a limiting factor in visualizing small vessels in the slice direction. Having a close to isotropic voxel size would have enabled the creation of 3D maps of the vasculature and also quantify blood oxygenation. All slices were acquired in the axial orientation relative to the magnetic axis. This resulted in images in oblique planes relative to the fetus, and was not consistent between fetuses, due to their varying orientation within the uterine horn. The voxel aspect ratio and the oblique orientation inhibited anatomical evaluation of the smaller structures. Another limitation of our study was that longitudinal evaluation of tissue property changes within the same placenta could not be performed. Although identification of the same fetus in longitudinal MRI examination is a challenge [75], such a study across gestation could help elucidate which of the placental regions contributes largely to the decrease in placental T2 relaxation with advancing gestational age.

Conclusions

Placental T2 relaxation times decrease with advancing gestational age in murine pregnancy which may reflect normal gestational-age dependent changes in placental perfusion. SWI can be

used to visualize embryonic vascular development early in gestation without using any exogenous contrast agents.

Acknowledgements

This research was supported, in part, by the Perinatology Research Branch, Division of Intramural Research, *Eunice Kennedy Shriver* National Institute of Child Health and Human Development (NICHD), National Institutes of Health (NIH), Department of Health and Human Services (DHHS); and, in part, with Federal funds from NICHD (NIH, DHHS) under Contract No. HHSN275201300006C. The authors are grateful to Dr. Theodore Price (Perinatology Research Branch), Dr. Lisa J. Brossia-Root, Laura Lee McIntyre, and all personal involved in the Division of Laboratory Animal Resources (Wayne State University). This work was also supported in part by a Small Business Technology Transfer (STTR) grant from the National Heart, Lung, and Blood Institute (NHLBI, NIH, DHHS; 1R42HL112580-01A1), by Wayne State University's Perinatal Research Initiative and Perinatology Virtual Discovery Grant to J.N. (made possible by the W.K. Kellogg Foundation award P3018205).

Disclosure/Conflicts of Interest

The authors have no conflicts of interest.

References:

1. Wildman, D.E., et al., *Evolution of the mammalian placenta revealed by phylogenetic analysis.* Proc Natl Acad Sci U S A, 2006. **103**(9): p. 3203-8.
2. Carter, A.M. and A. Mess, *Evolution of the placenta in eutherian mammals.* Placenta, 2007. **28**(4): p. 259-62.
3. Godfrey, K.M., *The role of the placenta in fetal programming-a review.* Placenta, 2002. **23 Suppl A**: p. S20-7.
4. Benirschke, K., P. Kaufmann, and R.N. Baergen, *Pathology of the human placenta*. Vol. 4. 2006: Springer.
5. Watson, E.D. and J.C. Cross, *Development of structures and transport functions in the mouse placenta.* Physiology (Bethesda), 2005. **20**: p. 180-93.
6. Than, N.G., et al., *A primate subfamily of galectins expressed at the maternal-fetal interface that promote immune cell death.* Proc Natl Acad Sci U S A, 2009. **106**(24): p. 9731-6.
7. Moffett, A. and C. Loke, *Immunology of placentation in eutherian mammals.* Nat Rev Immunol, 2006. **6**(8): p. 584-94.
8. Dilworth, M.R. and C.P. Sibley, *Review: Transport across the placenta of mice and women.* Placenta, 2013. **34 Suppl**: p. S34-9.
9. Longtine, M.S. and D.M. Nelson, *Placental dysfunction and fetal programming: the importance of placental size, shape, histopathology, and molecular composition.* Semin Reprod Med, 2011. **29**(3): p. 187-96.
10. Sibley, C.P., et al., *Placental phenotypes of intrauterine growth.* Pediatr Res, 2005. **58**(5): p. 827-32.
11. Redman, C.W., *Current topic: pre-eclampsia and the placenta.* Placenta, 1991. **12**(4): p. 301-8.
12. Damodaram, M., et al., *Placental MRI in intrauterine fetal growth restriction.* Placenta, 2010. **31**(6): p. 491-8.
13. Egbor, M., et al., *Pre-eclampsia and fetal growth restriction: how morphometrically different is the placenta?* Placenta, 2006. **27**(6): p. 727-734.
14. Huppertz, B., et al., *Placental morphology: from molecule to mother -- a dedication to Peter Kaufmann -- a review.* Placenta, 2006. **27 Suppl A**: p. S3-8.
15. Cetin, I. and P. Antonazzo, *The role of the placenta in intrauterine growth restriction (IUGR).* Z Geburtshilfe Neonatol, 2009. **213**(3): p. 84-8.
16. Benavides-Serralde, A., et al., *Changes in central and peripheral circulation in intrauterine growth-restricted fetuses at different stages of umbilical artery flow deterioration: new fetal cardiac and brain parameters.* Gynecologic and obstetric investigation, 2011. **71**(4): p. 274-280.
17. Barut, A., et al., *Placental chorangiosis: the association with oxidative stress and angiogenesis.* Gynecologic and obstetric investigation, 2012. **73**(2): p. 141-151.
18. McCarthy, F.P., et al., *Animal models of preeclampsia; uses and limitations.* Placenta, 2011. **32**(6): p. 413-9.
19. Elovitz, M.A. and C. Mrinalini, *Animal models of preterm birth.* Trends Endocrinol Metab, 2004. **15**(10): p. 479-87.
20. Harding, J.E., et al., *Animal studies of the effects of early nutrition on long-term health.* Nestle Nutr Workshop Ser Pediatr Program, 2011. **68**: p. 1-11; discussion 11-6.
21. Schwitzgebel, V.M., E. Somm, and P. Klee, *Modeling intrauterine growth retardation in rodents: Impact on pancreas development and glucose homeostasis.* Mol Cell Endocrinol, 2009. **304**(1-2): p. 78-83.

22. Georgiades, P., A.C. Ferguson-Smith, and G.J. Burton, *Comparative developmental anatomy of the murine and human definitive placentae.* Placenta, 2002. **23**(1): p. 3-19.
23. Rossant, J. and J.C. Cross, *Placental development: lessons from mouse mutants.* Nat Rev Genet, 2001. **2**(7): p. 538-48.
24. An, H., et al., *Evaluation of MR-derived cerebral oxygen metabolic index in experimental hyperoxic hypercapnia, hypoxia, and ischemia.* Stroke, 2009. **40**(6): p. 2165-72.
25. Bandettini, P.A., et al., *Spin-echo and gradient-echo EPI of human brain activation using BOLD contrast: a comparative study at 1.5 T.* NMR in Biomedicine, 1994. **7**(1-2): p. 12-20.
26. Wright, C., et al., *Magnetic resonance imaging relaxation time measurements of the placenta at 1.5 T.* Placenta, 2011. **32**(12): p. 1010-1015.
27. Gossuin, Y., P. Gillis, and F. Lo Bue, *Susceptibility-induced T2-shortening and unrestricted diffusion.* Magnetic resonance in medicine, 2002. **47**(1): p. 194-195.
28. Thulborn, K.R., et al., *Oxygenation dependence of the transverse relaxation time of water protons in whole blood at high field.* Biochimica et Biophysica Acta (BBA)-General Subjects, 1982. **714**(2): p. 265-270.
29. Muhler, M.R., et al., *Maternofetal pharmacokinetics of a gadolinium chelate contrast agent in mice.* Radiology, 2011. **258**(2): p. 455-60.
30. Alison, M., et al., *Measurement of Placental Perfusion by Dynamic Contrast-Enhanced MRI at 4.7 T.* Investigative radiology, 2013. **48**(7): p. 535-542.
31. Salomon, L.J., et al., *Placental Perfusion MR Imaging with Contrast Agents in a Mouse Model1.* Radiology, 2005. **235**(1): p. 73-80.
32. Bobek, G., et al., *Magnetic resonance imaging detects placental hypoxia and acidosis in mouse models of perturbed pregnancies.* PLoS One, 2013. **8**(3): p. e59971.
33. Duncan, K.R., et al., *The investigation of placental relaxation and estimation of placental perfusion using echo-planar magnetic resonance imaging.* Placenta, 1998. **19**(7): p. 539-43.
34. Kaufman, M.H. and J.B. Bard, *The anatomical basis of mouse development*. Vol. 28. 1999: Academic Press San Diego, CA:.
35. Turnbull, D.H. and S. Mori, *MRI in mouse developmental biology.* NMR Biomed, 2007. **20**(3): p. 265-74.
36. Parasoglou, P., et al., *High-resolution MRI of early-stage mouse embryos.* NMR Biomed, 2013. **26**(2): p. 224-31.
37. Degani, S., *Fetal cerebrovascular circulation: a review of prenatal ultrasound assessment.* Gynecologic and obstetric investigation, 2008. **66**(3): p. 184-196.
38. Zatik, J., et al., *Comparison of cerebral blood flow velocity as measured in preeclamptic, healthy pregnant, and nonpregnant women by transcranial Doppler sonography.* Gynecologic and obstetric investigation, 2001. **51**(4): p. 223-227.
39. Matsuda, Y., et al., *Cerebral magnetic resonance angiographic findings in severe preeclampsia.* Gynecologic and obstetric investigation, 1995. **40**(4): p. 249-252.
40. Reichenbach, J.R., et al., *High-resolution MR venography at 3.0 Tesla.* Journal of computer assisted tomography, 2000. **24**(6): p. 949-957.
41. Cho, Z., Y. Ro, and T. Lim, *NMR venography using the susceptibility effect produced by deoxyhemoglobin.* Magnetic resonance in medicine, 1992. **28**(1): p. 25-38.
42. Haacke, E.M., et al., *Susceptibility weighted imaging (SWI).* Magn Reson Med, 2004. **52**(3): p. 612-8.
43. Mittal, S., et al., *Susceptibility-weighted imaging: technical aspects and clinical applications, part 2.* AJNR Am J Neuroradiol, 2009. **30**(2): p. 232-52.
44. Haacke, E.M., et al., *Susceptibility-weighted imaging: technical aspects and clinical applications, part 1.* AJNR Am J Neuroradiol, 2009. **30**(1): p. 19-30.

45. Reichenbach, J.R., et al., *Small vessels in the human brain: MR venography with deoxyhemoglobin as an intrinsic contrast agent.* Radiology, 1997. **204**(1): p. 272-277.
46. Wu, Z., et al., *Identification of Calcification With MRI Using Susceptibility-Weighted Imaging: A Case Study.* Journal of Magnetic Resonance Imaging, 2009. **29**(1): p. 177-182.
47. Thomas, B., et al., *Clinical applications of susceptibility weighted MR imaging of the brain - a pictorial review.* Neuroradiology, 2008. **50**(2): p. 105-16.
48. Ashwal, S., et al., *Susceptibility-weighted imaging and proton magnetic resonance spectroscopy in assessment of outcome after pediatric traumatic brain injury.* Archives of Physical Medicine and Rehabilitation, 2006. **87**(12): p. S50-S58.
49. Lequin, M.H., et al., *Magnetic resonance imaging in neonatal stroke.* Seminars in Fetal & Neonatal Medicine, 2009. **14**(5): p. 299-310.
50. J. Neelavalli, S.M., L. Yeo, S. J. Korzekieski, S. Saleem, Y., P.K.J. Katkuri, R. O. Bahado-Singh, S. S. Hassan, H. EM, R., and R.a.M.E. Thomason, *Magnetic Resonance Venography Of The Fetal Brain Using Susceptibility Weighted Imaging*. 2013: Journal of Magnetic Resonance Imaging. p. In Press.
51. S. Mody, L.Y., J. Neelavalli, M. E. Thomason, E.Hernandez-Andrade, S. Hassan, R. Romero and H. E. M *Susceptibility weighted imaging of the fetal brain is superior to ultrasound and conventional MRI sequences in detecting intracranial hemorrhage*. in *Fourth International Congress on Fetal MRI.* . 2013. Ultrasound Obstet Gynecol.
52. *Guide for the Care and Use of Laboratory Animals: Eighth Edition*. 2011: The National Academies Press.
53. Yankeelov, T.E., et al., *Comparison of a reference region model with direct measurement of an AIF in the analysis of DCE-MRI data.* Magn Reson Med, 2007. **57**(2): p. 353-61.
54. Jenkinson, M., *Fast, automated, N-dimensional phase-unwrapping algorithm.* Magn Reson Med, 2003. **49**(1): p. 193-7.
55. Wang, Y., et al., *Artery and vein separation using susceptibility-dependent phase in contrast-enhanced MRA.* Journal of Magnetic Resonance Imaging, 2000. **12**(5): p. 661-670.
56. Haacke, E., et al., *Susceptibility-weighted imaging: technical aspects and clinical applications, part 1.* American Journal of Neuroradiology, 2009. **30**(1): p. 19-30.
57. Pinheiro, J. and D. Bates, *Mixed-effects models in S and S-PLUS Springer.* New York, 2000.
58. Wu, Z., et al., *Identification of calcification with MRI using susceptibility-weighted imaging: a case study.* Journal of Magnetic Resonance Imaging, 2009. **29**(1): p. 177-182.
59. Gillis, P. and S.H. Koenig, *Transverse relaxation of solvent protons induced by magnetized spheres: application to ferritin, erythrocytes, and magnetite.* Magnetic resonance in medicine, 1987. **5**(4): p. 323-345.
60. Brooks, R.A., F. Moiny, and P. Gillis, *On T2-shortening by weakly magnetized particles: the chemical exchange model.* Magn Reson Med, 2001. **45**(6): p. 1014-20.
61. Jensen, J. and R. Chandra, *NMR relaxation in tissues with weak magnetic inhomogeneities.* Magnetic resonance in medicine, 2000. **44**(1): p. 144-156.
62. Derwig, I., et al., *Association of placental T2 relaxation times and uterine artery Doppler ultrasound measures of placental blood flow.* Placenta, 2013. **34**(6): p. 474-9.
63. Raz, T., et al., *The hemodynamic basis for positional- and inter-fetal dependent effects in dual arterial supply of mouse pregnancies.* PLoS One, 2012. **7**(12): p. e52273.
64. Rennie, M.Y., et al., *Expansion of the fetoplacental vasculature in late gestation is strain dependent in mice.* American Journal of Physiology-Heart and Circulatory Physiology, 2012. **302**(6): p. H1261.
65. Chapon, C., et al., *In utero time-course assessment of mouse embryo development using high resolution magnetic resonance imaging.* Anatomy and Embryology, 2002. **206**(1-2): p. 131-137.

66. Berrios-Otero, C.A., et al., *Three-dimensional micro-MRI analysis of cerebral artery development in mouse embryos.* Magnetic Resonance in Medicine, 2009. **62**(6): p. 1431-1439.
67. Petiet, A.E., et al., *High-resolution magnetic resonance histology of the embryonic and neonatal mouse: a 4D atlas and morphologic database.* Proc Natl Acad Sci U S A, 2008. **105**(34): p. 12331-6.
68. Dhenain, M., S.W. Ruffins, and R.E. Jacobs, *Three-dimensional digital mouse atlas using high-resolution MRI.* Developmental Biology, 2001. **232**(2): p. 458-470.
69. Berrios-Otero, C.A., et al., *In utero phenotyping of mouse embryonic vasculature with MRI.* Magn Reson Med, 2012. **67**(1): p. 251-7.
70. Haacke, E.M. and J.R. Reichenbach, *Susceptibility weighted imaging in MRI: basic concepts and clinical applications*. 2011: Wiley. com.
71. Duyn, J.H., et al., *High-field MRI of brain cortical substructure based on signal phase.* Proceedings of the National Academy of Sciences, 2007. **104**(28): p. 11796-11801.
72. Xu, Y. and E.M. Haacke, *The role of voxel aspect ratio in determining apparent vascular phase behavior in susceptibility weighted imaging.* Magn Reson Imaging, 2006. **24**(2): p. 155-60.
73. Haacke, E., et al., *Susceptibility mapping as a means to visualize veins and quantify oxygen saturation.* Journal of Magnetic Resonance Imaging, 2010. **32**(3): p. 663-676.
74. J. Neelavalli, P.K.J., U. B. Krishnamurthy, S. Buch, H. EM, L.Yeo, S. Mody, Y. Katkuri, R. O. Bahado-Singh, S. S. Hassan, R. Romero and M. E. Thomaso, *Measuring Venous Blood Oxygenation in Fetal Brain using Susceptibility Weighted Imaging*. 2013: Journal of Magnetic Resonance Imaging 2013. p. In Press.
75. Avni, R., et al., *Unique in utero identification of fetuses in multifetal mouse pregnancies by placental bidirectional arterial spin labeling MRI.* Magnetic Resonance in Medicine, 2012. **68**(2): p. 560-570.
76. Jacobs, R.E., et al., *MRI: volumetric imaging for vital imaging and atlas construction.* Nat Rev Mol Cell Biol, 2003. **Suppl**: p. SS10-6.

Tables:

Table 1: Summary of MR imaging parameters in the murine model

Sequence	TE (in msec)	TR (in msec)	BW (in Hz/pixel)	In plane isotropic voxel size (in mm)	Slice thickness (in mm)
Multi echo spin Echo sequence	15,30,45,60,75,90 (or) 10.8, 21.6, 32.4, 43.2, 54, 64.8	2540-2840	130-150	0.08 - 0.13	0.7 - 0.8
SWI	5.42 - 7.84	600-850	150	0.08	0.7 - 0.8

Table 1: Summary of the MRI parameters used for multi echo spin echo T2 weighted imaging sequence (second row) and for SWI imaging sequence (third row). TE - echo time, TR - repetition time, BW – bandwidth, Hz – hertz, SWI – susceptibility weighted imaging.

Figures

Figure title

Figure 1. Murine placental T2 transverse relaxation times at different gestational ages

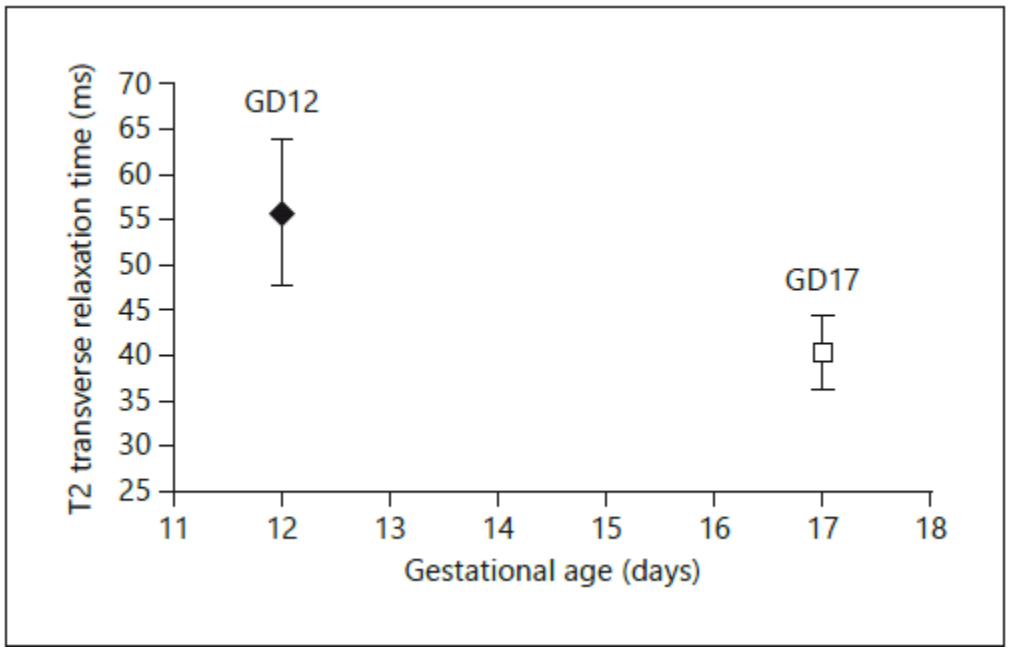

Figure legend

Figure 1: Plot of the T2 transverse relaxation time of the murine placenta on GD12 and GD17.

Figure title

Figure 2. Normalized plot of T2 murine placental transverse relaxation times at different gestational ages

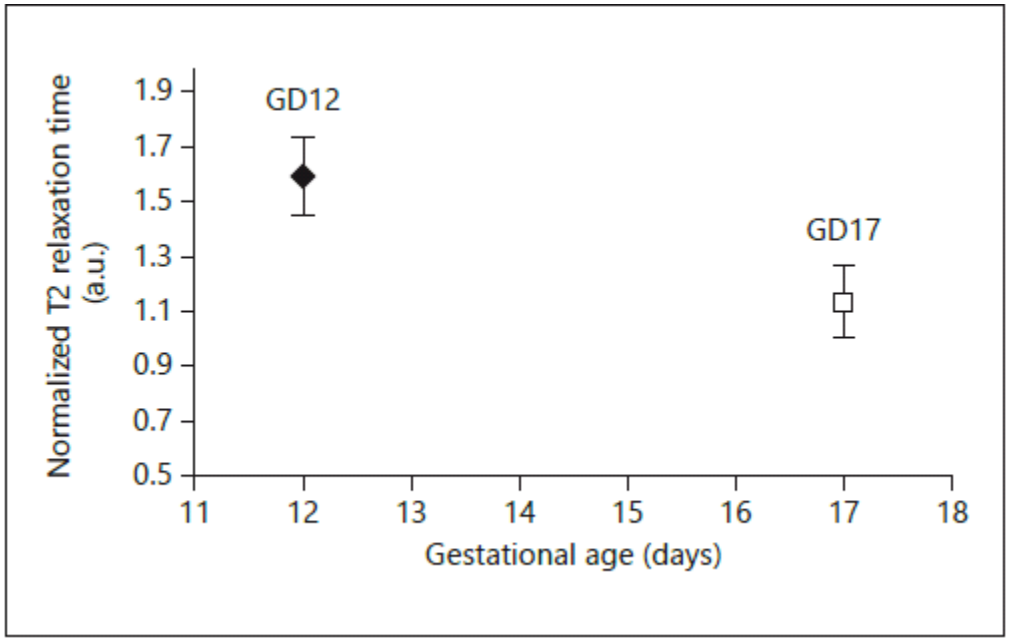

Figure legend

Figure 2: Plot of the normalized T2 transverse relaxation time of the murine placenta on GD12 and GD17 (represented in arbitrary units (a.u)). The maternal muscle T2 relaxation time value was used as the reference for normalization. Normalized values were computed as the ratio of placental T2 value / maternal muscle T2 value.

Figure title

Figure 3. SWI processed images showing the heterogeneity of the murine placenta on gestational day 12 and 17.

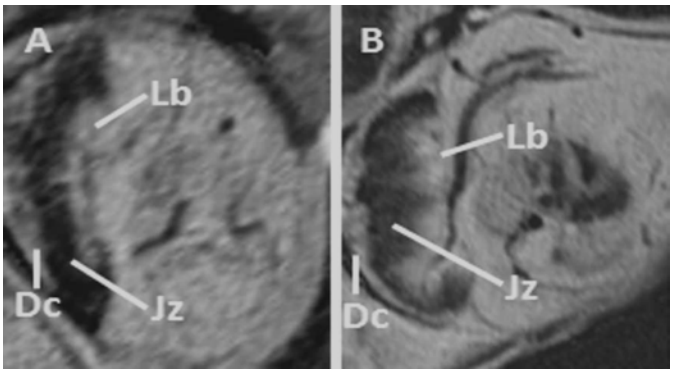

Figure legend

Figure 3: SWI processed image showing the heterogeneity of the murine placenta on GD12 (A) and GD17 (B) . Note the clear distinction between the three layers of the placenta: Lb – labyrinth, Jz - junctional zone, and Dc – decidua. GD – gestational day.

Figure title

Figure 4. SWI Venography: Processed SWI phase images of the fetus on gestational day 12.

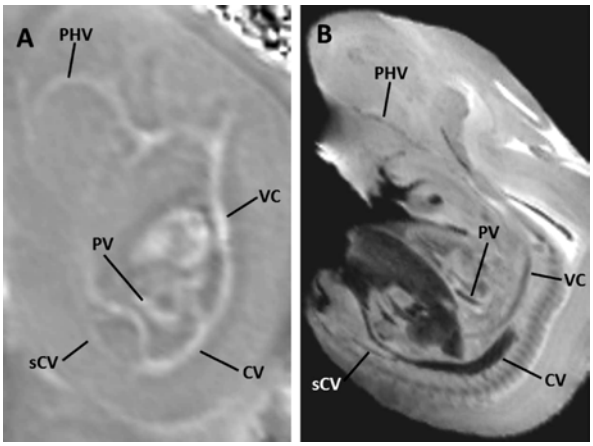

Figure legend

Figure 4: SWI processed phase image on GD12 (0.08x0.08x0.7 mm^3) (A), and the corresponding slice from high resolution minimum intensity projection (mIP) (B) (0.05x0.05x0.1 mm^3) adopted from the open source eMouse Atlas Project (EMAP) (http://www.emouseatlas.org) [68, 76]. Structures denoted by arrows are the followings: PHV - primary head vein, VC - vena cava, CV - cardinal vein, sCV - subcardial vein, and PV - portal vein.

Figure title

Figure 5. Processed SWI phase images of the fetus on gestational day 12.

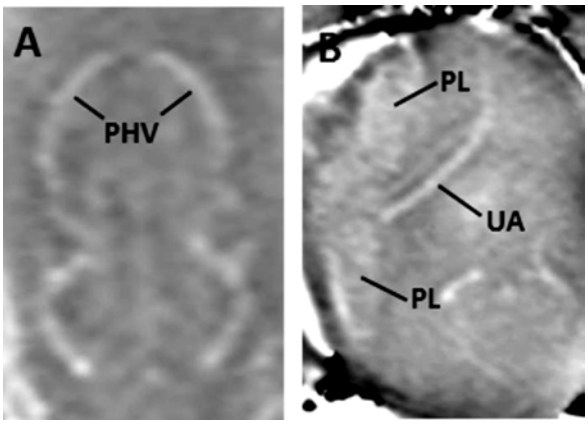

Figure legend

Figure 5: SWI processed phase images of different fetuses on GD12 (0.08x0.08x0.7 mm^3). The primary head vein (PHV in A), the placenta (PL in B) and the umbilical artery (UA in B) were clearly seen.

Figure title

Figure 6. SWI tissue contrast: Processed SWI phase images of the fetus on gestational day 17

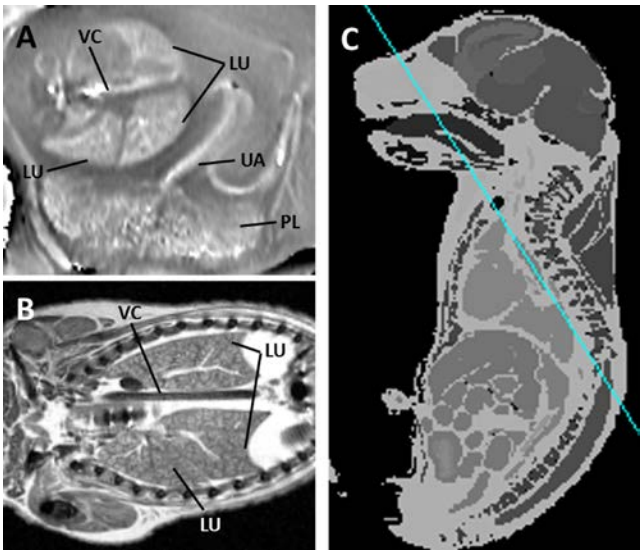

Figure legend

Figure 6: SWI processed phase image is shown on GD17 (0.08x0.08x0.7 mm3) (A). The corresponding slice from high resolution (0.058x0.058x0.58 mm3) atlas adopted from the Caltech open source (http://mouseatlas.caltech.edu/) [68, 76] (B-C). Different structures are shown as the followings: LU - lobes of the lungs, VC - vena cava, UA - umbilical artery, and PL - placenta.

Figure title

Figure 7. Visualization of bony structures: Processed SWI phase images of the fetus on gestational day 17

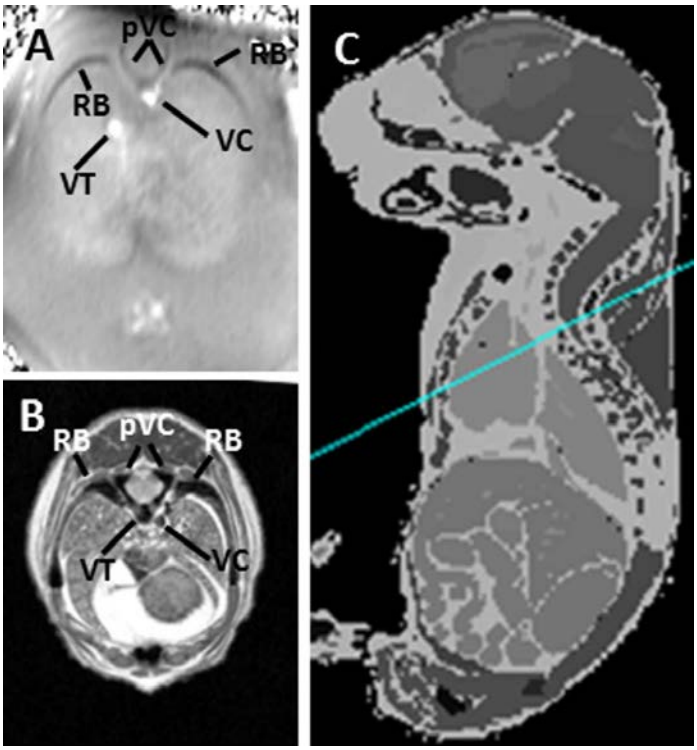

Figure legend

Figure 7: SWI processed phase image is shown on GD17 (0.08x0.08x0.7 mm^3) (A). The corresponding slice from a high resolution (0.058x0.058x0.58 mm^3) atlas adopted from the Caltech open source (http://mouseatlas.caltech.edu/) [68, 76] (B-C). Different structures are shown as the following: pVC - processes of the vertebral columns, RB - ribs, VC - vena cava, and other VT - veins in the thorax. Note the difference in the contrast between the veins and the bones.